Aspherical Supernova Explosions: Hydrodynamics, Radiation Transport & Observational Consequences

P. Höflich[1], A. Khokhlov [2], L. Wang[3]

[1] *Department of Astronomy, University of Texas, Austin, TX 78681, USA*
[2] *Naval Research Lab, Washington DC, USA*
[3] *Lawrence Berkeley Lab, 1 Cyclotron Rd, Berkeley, CA 94720, USA*

Abstract. Core collapse supernovae (SN) are the final stages of stellar evolution in massive stars during which the central region collapses, forms a neutron star (NS), and the outer layers are ejected. Recent explosion scenarios assumed that the ejection is due to energy deposition by neutrinos into the envelope but detailed models do not produce powerful explosions. There is new and mounting evidence for an asphericity and, in particular, for axial symmetry in several supernovae which may be hard to reconcile within the spherical picture. This evidence includes the observed high polarization and its variation with time, pulsar kicks, high velocity iron-group and intermediate-mass elements material observed in remnants, direct observations of the debris of SN1987A etc. Some of the new evidence is discussed in more detail. To be in agreement with the observations, any successful mechanism must invoke some sort of axial symmetry for the explosion.

As a limiting case, we consider jet-induced/dominated explosions of "classical" core collapse supernovae. The discovery of magnetars revived the idea that a MHD-jet with appropriate properties may be formed at the NS. Our study is based on detailed 3-D hydrodynamical and radiation transport models. We demonstrate the influence of the jet properties and of the underlying progenitor structure on the final density and chemical structure. Our calculations show that low velocity, massive jets can explain the observations. Both asymmetric ionization and density/chemical distributions have been identified as crucial for the formation of asymmetric photospheres. Even within the picture of jet-induced explosion, the latter effect alone fails to explain early polarization in core collapse supernovae with a massive, hydrogen-rich envelopes such as SN1999em. Finally, we discuss observational consequences and tests.

I OBSERVATIONAL EVIDENCE FOR ASYMMETRY

In recent years, there has been a mounting evidence that the explosions of massive stars (core collapse supernovae) are highly aspherical. (1) The spectra of core-collapse supernovae (e.g., SN87A, SN1993J, SN1994I, SN1999em) are significantly polarized indicating asymmetric envelopes by factors up to 2 (Méndez et al.

1988; Höflich 1991; Jeffrey 1991; Wang et al. 1996; Wang et al. 2001). The degree of polarization tends to vary inversely with the mass of the hydrogen envelope, being maximum for Type Ib/c events with no hydrogen (Wang et al. 2000). For SN1999em (Fig. 1), Leonard et al. (2000) showed that the polarization and, thus, the asphericity increases with time. Both trends suggest a connection of the asymmetries with the central engine. For supernovae with a good time and wavelength coverage, the orientation of the polarization vector tends to stay constant both in time and in the wavelength. This implies that there is a global symmetry axis in the ejecta (Leonard et al. 2001, Wang et al. 2001). (2) Observations of SN 1987A showed that radioactive material was brought to the hydrogen rich layers of the ejecta very quickly during the explosion (Lucy 1988; Tueller et al. 1991). (3) The remnant of the Cas A supernova shows rapidly moving oxygen-rich matter outside the nominal boundary of the remnant and evidence for two oppositely directed jets of high-velocity material (Fesen & Gunderson 1997). (4). Recent X-ray observations with the CHANDRA satellite have shown an unusual distribution of iron and silicon group elements with large scale asymmetries in Cas A (Huges et al. 2000). (5) After the explosion, neutron stars are observed with high velocities, up to 1000 km/s (Strom et al. 1995). (6) Direct HST-images from June 11,2000, are able to resolve the inner debris of SN1987A showing its prolate geometry with an axis ratio of ≈ 2 (Fig. 1). Both the ejecta and the inner ring around SN1987A show a common axis of symmetry. By combining the HST-images with spectral and early-time polarization data, Lifan Wang worked out the details of the chemical and density structure. By connecting the HST-images with the polarization data from earlier times, he demonstrated that the overall geometry of the entire envelope of SN1987A was elongated all along the symmetry axis (including the H-rich envelope), and that the distribution of the products of stellar burning products (O, Ca, etc.) are concentrated in the equatorial plane (Wang et al. 2001).

II   MODELS FOR COLLAPSE SUPERNOVA

There is a general agreement that the explosion of a massive star is caused by the collapse of its central parts into a neutron star or, for massive progenitors, into a black hole. The mechanism of the energy deposition into the envelope is still debated. The process likely involves the bounce and the formation of the prompt shock (e.g. Van Riper 1978, Hillebrandt 1982), radiation of the energy in the form of neutrinos (e.g. Bowers & Wilson 1982), and the interaction of the neutrino with the material of the envelope and various types of convective motions (e.g. Herant et al. 1994, Burrows et al. 1995, Müller & Janka 1997, Janka & Müller 1996), rotation (e.g. LeBlanc & Wilson 1970, Saenz & Shapiro S.L. 1981, Mönchmeyer et al. 1991, Zwerger & Müller 1997) and magnetic fields (e.g. LeBlanc & Wilson 1970, Bisnovati-Kogan 1971).

Currently, the most favored mechanism invokes the neutrino deposition. The results depend critically on the progenitor structure, equation of state, neutrino
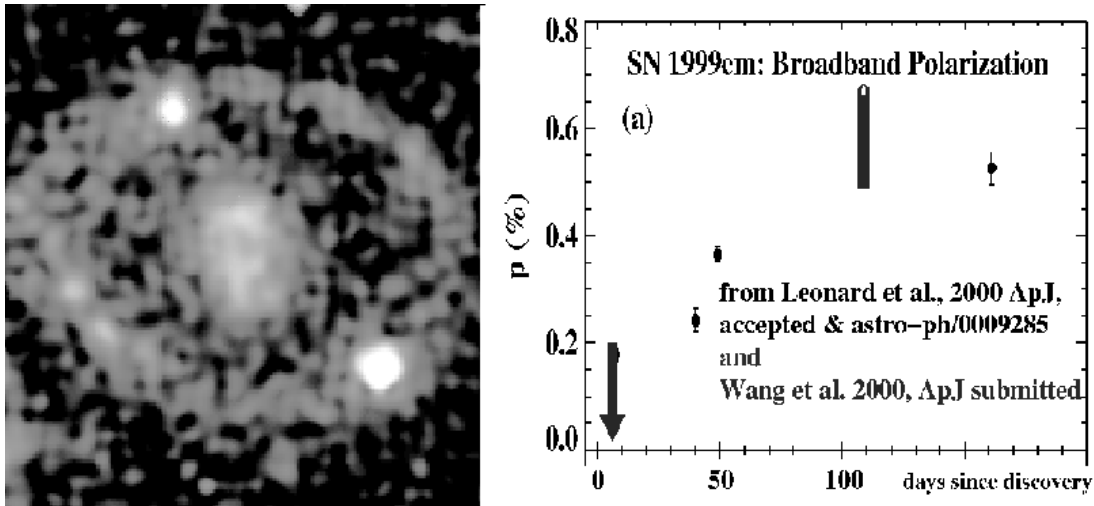
FIGURE 1. Observational evidence for asphericity in core collapse supernovae. The HST image of SN 1987A (left panel) shows the inner debris of the SN-ejecta with an axis ratio of ≈ 2 and the ring on June 11th, 2000 (from Wang et al. 2001). Note that the inner ring has been formed during the stellar evolution about 10,000 years before the explosion. The right panel shows the evolution with time of the linear polarization P in the plateau supernovae SN1999em. Although P increased with time, the polarization angle remained constant with time and wavelength indicating a common axis of symmetry in the expanding envelope (Leonard et al. 2001, Wang et al. 2001).

physics, and implementation of the neutrino transport. Recent results indicate that spherical models fail to produce successful explosions even when using sophisticated, relativistic Boltzmann solvers for the neutrino transport and taking different flavors and neutrinos into account (Yamada et al. 1999, Ramp & Janka 2000, Mezzacappa et al. 2001). Multi-dimensional effects such as convection during the core collapse itself must be included but, still, it is an open question whether convection combined with the neutrino transport provides the solution to the supernova problem (Ramp et al. 1998 and references therein). In the current calculations, the size and scale of the convective motions seem to be too small to explain the observed asymmetries in the envelope. The angular variability of the neutrino flux caused by the convection has been invoked to explain the neutron star kicks (Burrows et al. 1995, Janka & Müller 1994). Calculations give kick velocity up to $\simeq 100$ km/s whereas NS with velocities of several 100 km/s are common. For a more detailed discussion of the current status and problems to explain the observed asymmetries, see Khokhlov & Höflich (2001).

It has long been suggested that the magnetic field can play an important role in the explosion (LeBlanc & Wilson 1970; Ostriker & Gunn 1971, Bisnovati-Kogan 1971, Symbalisty 1984). LeBlanc and Wilson simulations showed the amplification of the magnetic field due to rotation and the formation of two oppositely directed, high-density, supersonic jets of material emanating from the collapsed core. Their simulations assumed a rather high initial magnetic field $\sim 10^{11}$ Gauss and produced a very strong final fields of the order of $\sim 10^{15}$ Gauss which seemed to be

unreasonable at the time. The recent discovery of pulsars with very high magnetic fields (Kouveliotou et al. 1998, Duncan & Thomson 1992) revives the interest in the role of rotating magnetized neutron stars in the explosion mechanism. It is not clear whether a high initial magnetic field required for the LeBlanc & Wilson mechanism is realistic. On the other hand it may not be needed.

The current picture of the core collapse process is unsettled. A quantitative model of the core collapse must eventually include all the elements mentioned above.

Due to the difficulty of modeling core collapse from first principles, a very different line of attack on the explosion problem has been used extensively and proved to be successful in understanding of the supernova problem, SN1987A in particular (Arnett et al. 1990, Hillebrand & Höflich 1991). The difference of characteristic time scales of the core (a second or less) and the envelope (hours to days) allows one to divide the explosion problem into two largely independent parts - the core collapse and the ejection of the envelope. By assuming the characteristics of the energy deposition into the envelope during the core collapse, the response of the envelope can be calculated. Thus, one can study the observational consequences of the explosion and deduce characteristics of the core collapse and the progenitor structure. This approach has been extensively applied in the framework of the 1D spherically symmetric formulation. The major factors influencing the outcome have been found to be the explosion energy and the progenitor structure. The same approach can be applied in multi-dimensions to investigate the effects of asymmetric explosions. In this paper we study the effects and observational consequences of an asymmetric, jet-like deposition of energy inside the envelope of SN.

III   RESULTS FOR JET-INDUCED SUPERNOVAE

A   Numerical Methods

3-D Hydrodynamics: The explosion and jet propagation are calculated by a full 3-D code within a cubic domain. The stellar material is described by the time-dependent, compressible, Euler equations for inviscid flow with an ideal gas equation with $\gamma = 5/3$ plus a component due to radiation pressure with $\gamma = 4/3$. The Euler equations are integrated using an explicit, second-order accurate, Godunov type, adaptive-mesh-refinement, massively parallel, Fully-Threaded Tree (FTT) program, ALLA (Khokhlov 1998).

1-D Radiation-Hydrodynamics: About 1000 seconds after the core collapse and in case of the explosion of red supergiants, the propagation of the shock front becomes almost spherical (see below). To be able to follow the development up to the phase of homologous expansion ($\approx 3 - 5$ days), the 3-D structure is remapped on a 1-D grid, and the further evolution is calculated using a one-dimensional radiation-hydro code that solves the hydrodynamical equations explicitly in the comoving frame by the piecewise parabolic method (Colella and Woodward 1984).

The radiation transport part is solved implicitly using the method of variable Eddington factors. Expansion opacities and LTE-equations of state are used (Höflich et al. 1998 and references therein).

3-D Radiation Transport for Ionization Structures and Light Curves: For given, arbitrary 3-D density, velocity and chemical distributions, we calculated the detailed 3-D ionization structure and LCs using the same assumptions as for our 1-D hydro code. The γ-ray transport is computed in 3-D using a Monte Carlo method (Höflich et al. 1992, 1993) which includes relativistic effects and a consistent treatment of both the continua and line opacities. Subsequently, for low energy photons, we solve the three-dimensional radiation transport using a hybrid scheme of Monte-Carlo and non-equilibrium diffusion methods. As a first step, we solve the time-dependent radiation transport equation in non-equilibrium, diffusion approximation for 3-D geometry including the scattering and thermalization terms for the source functions, and include the frequency derivatives into the formulation for the opacities and emissivities. We solve the same set of momentum equations as Höflich et al. (1993) but for 3-D geometry and an Eddington factor of 1/3. At large optical depths, this provides the solution for the full radiation transport problem. In a second step, to obtain the correction solution for the radiation transport equation at small optical depths, the difference between the solution of the diffusion and full radiation transport equation is calculated in a Monte Carlo scheme. We calculate the difference between the solutions for computational accuracy and efficiency. Consistency between the solution at the outer and inner region is obtained iteratively. The same Monte Carlo solver is used which has been applied to compute γ-ray and polarization spectra. For simplification, the relation between energy density and temperature is taken from the 1-D radiation hydrodynamics at the corresponding time (see below).

3-D Radiation for Spectra and Polarization: For several moments of time, detailed polarization and flux spectra for asymmetric explosions are calculated using our MC-code including detailed equations of state, and detailed atomic models for some of the ions. For details, see Höflich (1995), Höflich et al. (1995) and Wang et al. (1998).

B   Jet propagation:

The Setup: The computational domain is a cube of size L with a spherical star of radius R_{star} and mass M_{star} placed in the center. The innermost part with mass $M_{\mathrm{core}} \simeq 1.6 M_\odot$ and radius $R_{\mathrm{core}} = 4.5 \times 10^8$ cm, consisting of Fe and Si, is assumed to have collapsed on a timescale much faster than the outer, lower-density material. It is removed and replaced by a point gravitational source with mass M_{core} representing the newly formed neutron star. The remaining mass of the envelope M_{env} is mapped onto the computational domain. At two polar locations where the jets are initiated at R_{core}, we impose an inflow with velocity v_j ρ_j. At R_{core}, the jet density and pressure are the same as those of the background material. For the
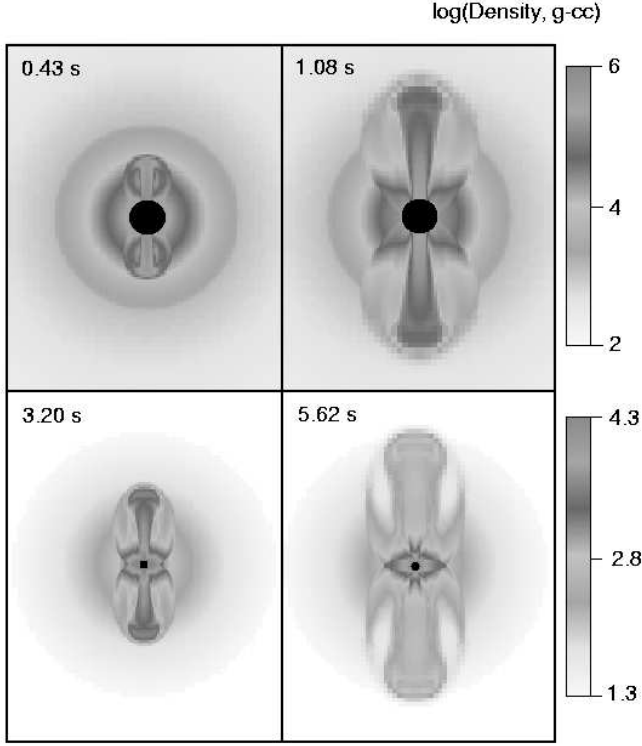
FIGURE 2. Logarithm of the density structure as a function of time for a helium core. The total mass of the ejecta is 2.6 $M_\odot$. The initial radius, velocity and density of the jet were taken to 1200 km 32,000 km/sec and $6.5E5 g/cm^3$, respectively. The shown domains 7.9, 9.0, 36 and $45 \times 10^9 cm$. The total energy is about 9E50 erg. After about 4.5 seconds, the jet penetrates the star. The energy deposited in the stellar envelope by the jet is about 4E50 erg, and the final asymmetry is of the order of two.

first 0.5 s, the jet velocity at R_{core} is kept constant at v_j. After 0.5 s, the velocity of the jets at R_{core} was gradually decreased to zero at approximately 2 s. The total energy of the jets is E_j. These parameters are consistent within, but somewhat less than, those of the LeBlanc-Wilson model.

The reference model: As a baseline case, we consider a jet-induced explosion in a helium star. Jet propagation inside the star is shown in Fig. 2. As the jets move outwards, they remain collimated and do not develop much internal structure. A bow shock forms at the head of the jet and spreads in all directions, roughly cylindrically around each jet. The jet-engine has been switched off after about 2.5 seconds the material of the bow shock continues to propagate through the star. The stellar material is shocked by the bow shock. Mach shocks travels two wards the equator resulting in a redistribution of the energy. The opening angle of the jet depends on the ratio between the velocity of the bow shock to the speed of sound. For a given star, this angle determines the efficiency of the deposition of the jet energy into the stellar envelope. Here, the efficiency of the energy deposition is

about 40 %, and the final asymmetry of the envelope is about two.

Influence of the jet properties: Fig. 3 shows two examples of an explosion with with a low and a very high jet velocity compared to the baseline case (Fig. 2). Fig. 3 demonstrates the influence of the jet velocity on the opening angle of the jet and, consequently, on the efficiency of the energy deposition. For the low velocity jet, the jet engine is switched off long before the jet penetrates the stellar envelope. Almost all of the energy of the jet goes into the stellar explosion. On a contrary, the fast jet (61,000 km/sec) triggers only a weak explosion of 0.9 foe although its total energy was $\approx 10\, foe$.

Influence of the progenitor: For a very extended star, as in case of 'normal' Type II Supernovae, the bow shock of a low velocity jet stalls within the envelope, and the entire jet energy is used to trigger the ejection of the stellar envelope. In our example (Fig. 5), the jet material penetrates the helium core at about 100 seconds. After about 250 seconds the material of the jet stalls within the hydrogen rich envelope and after passing about 5 solar masses in the radial mass scale of the spherical progenitor. At this time, the isobars are almost spherical, and an almost spherical shock front travels outwards. Consequently, Strong asphericities are limited to the inner regions. After about 385 seconds, we stopped the 3-D run and remaped the outer layers into 1-D structure, and followed the further evolution in 1-D. After about 1.8E4 seconds, the shock front reaches the surface. After about 3 days, the envelope expands homologously. The region where the jet material stalled, expands at velocities of about 4500 km/sec.

Fallback: Jet-induced supernovae have very different characteristics with respect to fallback of material and the innermost structure. In 1-D calculations and for stars with Main Sequence Masses of less than 20 $M_\odot$ and explosion energies in excess of 1 foe, the fallback of material remains less than 1.E-2 to 1.E-3 $M_\odot$ and an inner, low density cavity is formed with an outer edge of ^{56}Ni. For explosion energies between 1 and 2 foe, the outer edge of the cavity expands typically with
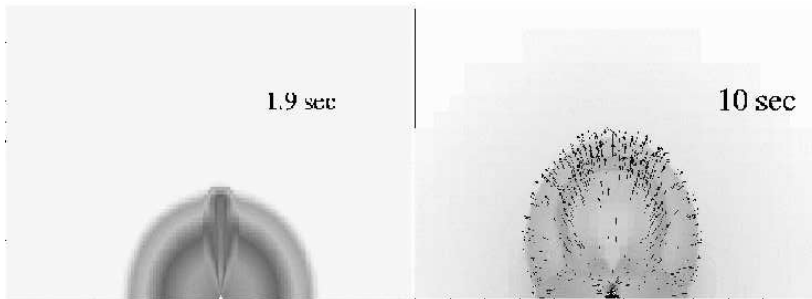

FIGURE 3. Same as Fig. 2 ($0.5 \leq log(\rho) \leq 5.7$) but for a jet velocity of 61,000 km/sec and a total energy of 10 foe at $\approx 1.9sec$ (left), and 11,000 km/sec and a total energy of 0.6 foe (right). The size of the presented domains are 5 (left) and 2 $10^{10}cm$ (right), respectively. For the high velocity jet, most of the energy is carried away by the jet. Only 0.9 foe are deposited in the expanding envelope. In case of a low velocity jet, the bow-shock still propagates through the star after the jet is switched off, and the entire jet energy is deposited in the expanding envelope.

velocities of about 700 to 1500 km/sec (e.g. Woosley 1997, Höflich et al. 2000). In contrast, we find strong, continuous fallback of $\approx 0.2 M_\odot$ in the the 3-D hydro models, and no lower limit for the velocity of the expanding material (Fig. 4 of Khokhlov & Höflich 2001). This significant amount of fallback must have important consequences for the secondary formation of a black hole. The exact amount and time scales for the final accretion on the neutron star will depend sensitively on the rotation and momentum transport.

Chemical Structure: The final chemical profiles of elements formed during the stellar evolution such as He, C, O and Si are 'butterfly- shaped' whereas the jet material fills an inner, conic structure (Fig. 5, upper, middle panel).

The composition of the jets must reflect the composition of the innermost parts of the star, and should contain heavy and intermediate-mass elements, freshly synthesized material such as ^{56}Ni and, maybe, r-process elements because, in our examples, the entropy at the bow shock region of the jet was as high as a few hundred. In any case, during the explosion, the jets bring heavy and intermediate mass elements into the outer H-rich layers.

C   Radiation Transport Effects

For the compact progenitors of SNe Ib/c, the final departures of the iso-density contours from sphericity are typical a factor of two. This will produce a linear polarization of about 2 to 3 % (Fig. 4) consistent with the values observed for Type Ib/c supernovae. In case of a red supergiant, i.e. SNe II, the asphericity is restricted to the inner layers of the H-rich envelope. There the iso-densities show an axis ratios of up to ≈ 1.3. The intermediate and outer H-rich layers
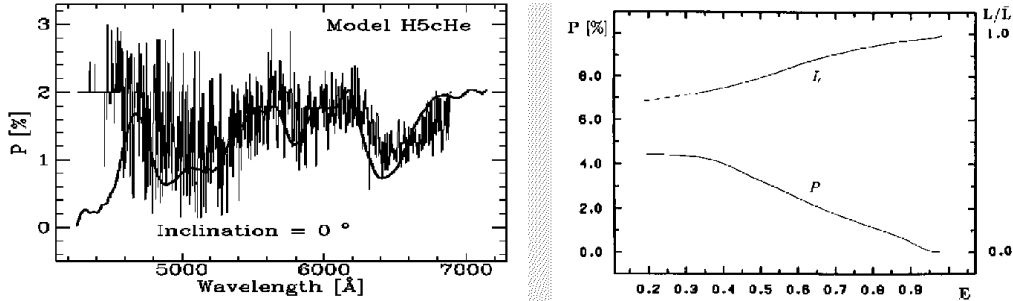

FIGURE 4. Polarization spectrum for SN1993J for an axis ratio of 1/2 for an oblate ellipsoid in comparison with observations by Trammell et al. (1993) are given in the left plot. On the right, the dependence of the continuum polarization (right) and directional dependence of the luminosity is shown as a function axis ratios for oblate ellipsoids seen from the equator (from Höflich, 1991 & Höflich et al. 1995).

remain spherical. This has strong consequences for the observations, in particular, for polarization measurements. In general, the polarization should be larger in SNe Ib/c compared to classical SNe II which is consistent with the observations by Wang et al. (2000). Early on, we expect no or little polarization in supernovae

with a massive, hydrogen rich envelope which will increase with time to about 1% (Höflich 1991), depending on the inclination the SN is observed. This is also consistent both with the long-term time evolution of SN1987A (Jefferies 1991).

Recently, the plateau supernova 1999em has been observed with VLT and Keck providing the best time coverage up to know of any supernovae (Wang et al. 2000; Leonard et al. 2001). The basic trend has been confirmed which we expected from the hydro. Indeed, P is very low early on, and it rises when more central parts are seen. However, there are profound differences which point towards an additional mechanism to produce aspherical photospheres.
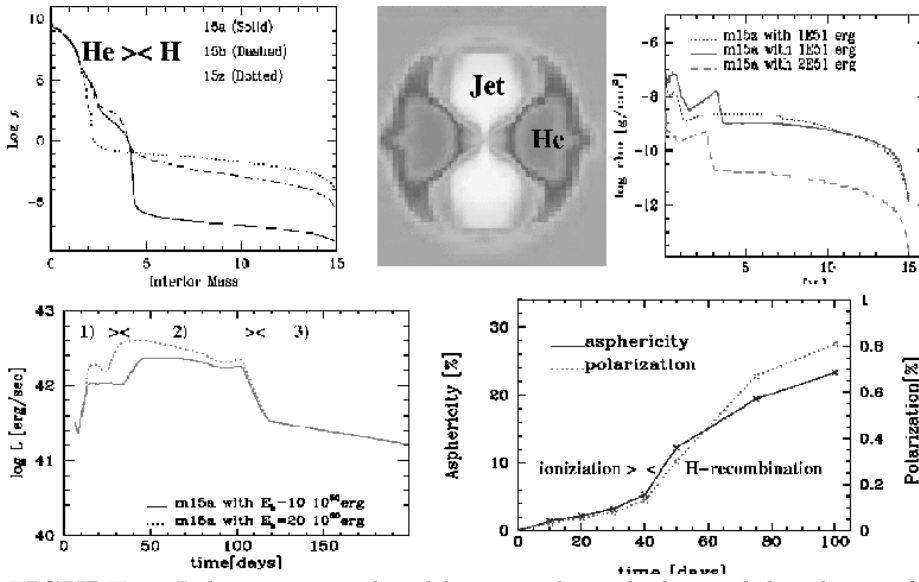

FIGURE 5. Polarization produced by an aspherical, chemical distribution for a SN IIp model with $15M_\odot$ and an explosion energy $E_{exp} = 2 \times 10^{51} erg$. This model resembles SN 1999em (see above). The initial density profile is given for a star at the final stage of stellar evolution for metallicities Z of 0.02, 0.001 and 0 (models 15a, 15b, 15z, upper left panel, from Höflich et al. 2000 & Chieffi et al. 2001). The model for the Red Supergiant, 15a, has been used to calculation of the jet-induced explosion in sect. 2). In the upper, middle panel, the chemical distribution of He is given at 250 sec for the He-rich layers after the jet material has stalled. The color-codes white, yellow, green, blue and red correspond to He mass fractions of 0., 0.18, 0.36, 0.72, and 1., respectively. The subsequent explosion has been followed in 1-D up to the phase of homologous expansion. In the upper, right panel, the density distribution is given at about 5 days after the explosion. The steep gradients in the density in the upper right and left panels are located at the interface between the He-core and the H-mantel. In the lower, left panel, the resulting bolometric LCs are given for a our $E_{exp} = 2 \times 10^{51} erg$ (dotted line) and, for comparison, for $1 \times 10^{51} erg$, respectively. Based on full 3-D calculations for the radiation & γ-ray transport, we have calculated the location of the recombination front as a function of time. The resulting shape of the photosphere is always prolate. The corresponding axis ratio and the polarization seen from the equator are shown (lower, right panel). Note the strong increase of the asphericity after the onset of the recombination phase between day 30 to 40 (see also SN 1999em in Fig. 1).

SN1999em is an extreme plateau supernovae with a plateau lasting for more than 100 days (IAUC 7294 to 7355). However, no detailed light curves have been published. Therefore, in Fig. 5, we show a theoretical LC which resembles SN 1999em with respect to the duration of the plateau and its brightness, and the typical expansion velocities. The light curves of SNe IIp show three distinct phases (Fig. 5). 1) Most of the envelope is ionized. This phase depends sensitively on the explosion energy, mixing of radioactive Ni, and the mass of the progenitor, e.g. either strong mixing or $E_{kin} \leq 1 foe$ will cause a steep and steady increase in the luminosity (and in B and V); 2) The emitted energy is determined by the receding (in mass) of the H recombination front which is responsible for both the release of stored, thermal and the recombination energy. At the recombination front, the opacity drops by about 3 orders of magnitude when it changes from electron scattering dominated to bound-free/ free-free. This provides a self regulating mechanism for the energy release. If too little energy is released, the opacity drops fast causing an increase in the speed at which the the photosphere is receding. In term, this causes a larger energy release and vs. . Hydrogen recombines at a specific temperature at or just below the photosphere. Due to the flat density profiles of the expanding envelopes in the RSG case, the photospheric radius and, thus, the luminosity L stays almost constant. After the recombination front has passed through the H-rich envelope, the brightness drops fast. During phase 3), L is given by the instant energy release by radioactive decay of ^{56}Co. Obviously, the steep rise in P of SN1999em coincide with the transition from phase 1 to 2, pointing towards un-isotropic excitation as a new mechanism for producing aspherical photospheres and, consequently, polarization. To quantify the effect, we have calculated the temperature and ionization structure of a SN IIp (Fig. 5). Starting from a spherical model, the initial chemical distribution has been taken from our 3-D jet simulation. As mentioned above, the chemical profile is frozen out after about 250 sec, and the expansion becomes spherical. The further evolution can be followed with our 1-D radiation code. For several moments of time, we have calculated the ionization structure and continuum polarization based of the 3-D chemical structure and the spherical density distribution under the assumption that the distribution of the radioactive Ni coincides with the jet-material. Note that the ^{56}Ni layers extend throughout the He-core ($\approx 5 M_\odot$) in polar directions but they are confined to the very center along the equatorial plane (Fig. 5, upper, middle panel) leading to an increased transport of energy and, consequently, heating toward polar directions. Before the recombination phase, the opacity is dominated by Thomson scattering which does not depend on the temperature, and the shape of the photosphere remains almost spherical. However, during the recombination phase, the location of the photosphere depends sensitively on the heating, and the photosphere becomes prolate (Fig. 5, lower, right panel). There is a gradual increase in P and no jump P because of the optically thick H-rich layers below the photosphere redistribute the photons. The increase of P depends on the geometrical expansion and speed (in mass) of the receding recombination front.

IV CONCLUSIONS

We have numerically studied the explosion of Core Collapse supernovae caused by supersonic jets generated in the center of the supernova as a result of the core collapse into a neutron star. We simulated the process of the jet propagation through the star, the redistribution of elements, and radiation transport effects. A strong explosion and a high efficiency for the conversion of the jet energy requires low jet velocities or a low, initial collimation of the jet. With increasing extension of the envelope, the conversion factor increases. Typically, we would expect higher kinetic energies in SNe II compared to SNe Ib/c if a significant amount of explosion energy is carried away by jets. Within the framework of jet-induced SN, the lack of this evidence suggests that the jets have low velocities.

The He, C, O and Si rich layers of the progenitor show characteristic, butterfly-shape structures. This overall morphology and pattern should be observable in supernovae remnants, e.g. with the Chandra observatory despite some modifications and instabilities when the expanding medium interacts with the interstellar material.

During the explosion, the jets bring heavy and intermediate mass elements into the outer layers including ^{56}Ni. Due to the high entropies of the jet material close to the center, this may be a possible site for r-process elements. Spatial distribution of the jet material will influence the properties of a supernova. In our model for a SN II, the jet material stalled within the expanding envelope corresponding to a velocity of $\approx 4500 km/sec$ during the phase of homologous expansion. In SN1987A, a bump in spectral lines of various elements has been interpreted by material excited by a clump of radioactive ^{56}Ni (Lucy 1988). Within our framework, this bump may be a measure of region where the jet stalled. This could also explain the early appearance of X-rays in SN1987A which requires strong mixing of radioactive material into the hydrogen-rich layers (see above), and the overall distribution of elements and distribution of elements in the resolved HST-images of the inner debris of SN 1987A. We note that, if this interpretation is correct, the 'mystery spot' (Nisenson et al. 1988) would be unrelated. In contrast to 1-D simulations, we find in our models strong, continuous fallback over an extended period of time, and a lack of an inner, almost empty cavity. This significant amount of fallback and the consequences for the secondary formation of a black hole shall be noted. Moreover, fallback and the low velocity material may alter the escape probability for γ-rays produced by radioactive decay of ^{56}Ni. In general, the lower escape probability is unimportant for the determination of the total ^{56}Ni production by the late LCs because full thermalization can be assumed in core collapse SN during the first few years. However, in extreme cases such as SN98BW (e.g. Schaefer et al. 2000), only a small fraction of gamma's are trapped. Effects of multi-dimensionality will strongly alter the energy input by radioactive material and disallow a reliable estimate for the total ^{56}Ni mass.

Qualitatively, the jet-induced picture allows to reproduce the polarization observed in core collapse supernovae. Both asymmetric ionization and den-

sity/chemical distributions have been identified as crucial. Even within the picture of jet-induced explosion, the latter effect alone cannot (!) account for the high polarization produced in the intermediate H-rich layers of core-collapse SN with a massive envelope such as SN 1999em. The former effect operates only during a recombination phase, and can be expected to dominate the polarization in core-collapse supernovae with massive H-rich envelope during the first 1 to 2 months. Complete time series of polarization measurements are needed to test this suggestion.

Finally, we want to emphasize the limits of this study and some of the open questions which will be addressed in future. We have assumed that jets are formed in the course of the formation of a neutron star, and have addressed observational consequences and constrains. However, we have not calculated the jet formation, we do not know if they really form, and, if they form, whether they form in all core-collapse supernovae. Qualitatively, the observational properties of core collapse supernovae are consistent with jet-induced supernovae and support strongly that the explosion mechanism is highly aspherical but more detailed comparisons with an individual objects must be performed as soon as the data become available. We cannot claim that the jets are the only mechanism that can explain asphericity in supernovae but any competing mechanism must involve some sort of axial symmetry on large scales with a profound impact on the explosion such as rapid rotation. It remains to be seen whether asymmetry and axial symmetry are the 'smoking gun' for our understanding of the SN-mechanism. mm

REFERENCES

1. Arnett W.D., Bahcall J.N., Kirshner, R.P., Woosley, S.E. 1990, ARAA 27, 62]bibitemBisnovatyi-Kogan 1971, Soviet Astronomy AJ, 14, 652
2. Bowers R.L., Wilson J.R. 1982 ApJS 50, 115
3. Burrows A., Hayes J., Fryxell B. 1995, ApJ 450
4. Colella, P.; Woodward, P.R. 1984, J.Comp.Phys. 54, 174
5. Duncan, R. C. & Thompson, C. 1992, ApJ, 392, L9
6. Fesen, R. A. & Gunderson, K. S. 1996, ApJ, 470, 967
7. Herant M., Benz W., Hix W.R., Fryer C.L., Colgate S.A. 1994, ApJ 435, 339
8. Hillebrandt W., Höflich 1991, Nuclear Physics B 19, 113
9. Hillebrandt W. 1982, ApJ 103, 147
10. Höflich P., Straniero O., Limongi M. Dominguez I. Chieffi A. 2000, 7th TexMex-Conference, eds. W. Lee & S. Torres-Peimbert, UNAM-Publ., in press & astro-ph/005037
11. Höflich, P., Wheeler, J. C., and Thielemann, F.K. 1998, ApJ 495, 617
12. Höflich, P. 1995, ApJ 443, 89

13. Höflich P., Wheeler, J.C., Hines, D., Trammell S. 1995, ApJ 459, 307
14. Höflich, P., Müller E., Khokhlov A. 1993, A&A 268, 570
15. Höflich, P., Müller E., Khokhlov A. 1992, A&A 259, 243
16. Höflich, P. 1991 A&A 246, 481
17. Huges J.P., Rakowski C.E., Burrows D.N., Slane P.O. 2000, AJ, in press & astro-ph/9910474
18. Janka H.T. & Müller E., 1994 A&A 290, 496
19. Jeffrey D.J., 1991, ApJ, 375, 264
20. Khokhlov A., Höflich P., Oran E.S., Wheeler J.C., P. Wang L., 1999, ApJ 524, L107
21. Khokhlov A.M., Höflich P. 2001, in: 1st KIAS Astrophysics, IAP-Publishing, ed. I. Yi, in press & astro-ph/0011023
22. Khokhlov, A.M. 1998, J.Comput.Phys., 143, 519
23. Kouveliotou, C., Strohmayer, T., Hurley, K., Van Paradijs, J., Finger, M. H., Dieters, S., Woods, P., Thompson, C. & Duncan, R. C. 1998, ApJ, 510, 115
24. Lucy L.B. 1988, Proc. of the 4th George Mason conference, ed. by M. Kafatos, Cambridge University Press, p. 323
25. LeBlanc, J. M. & Wilson, J. R. 1970, ApJ, 161, 541
26. Leonard D.C., Filippenko, A.V., Barth A.J., Matheson T. 2000, ApJ 536, 239
27. Mendez R.H., Clocchiatti A., Benvenuto O.G., Feinstein C. Marraco H. 1977, ApJ 334, 295
28. Mezzacappa A., Liebendoerfer M., Bronson Messer O.E. Hix R., Thielemann F-K, Bruenn S.W. 2001, Phy.Rev.Let., accepted
29. Mönchmeyer R., Schaefer G., Mueller E., Kates R.E. 1991 A&A 246, 417
30. Müller E., Janka H.T. 1997, A&A 317, 140
31. Nisenson P., Papaliolios C., Karovska M., Noyes R. 1988, ApJ 324, 35
32. Ostriker, J. P. & Gunn, J. E. 1971, ApJ, 164, L95
33. Rammp M., Müller E., Ruffert M. 1998, A&A 332, 969
34. Ramp M. and Janka, H.-T. 2000, ApJ 593, L33
35. Schaefer B. 2000, ApJ 533, 21
36. Saenz R.A., Shapiro S.L. 1981, ApJ 244, 1033
37. Symbalisty E.M.D. 1984, ApJ 285, 729
38. Strom R., Johnston H.M., Verbunt F., Aschenbach B. 1995, Nature, 373, 587
39. Symbalisty E.M.D. 1984, ApJ 285, 729
40. Trammell S., Hines D., Wheeler J.C. 1993, ApJ 414, 21
41. Tueller J., Barthelmy S., Gehrels N., Leventhal M., MacCallum C.J., Teegarden B.J. 1991, in: Supernovae, ed. S.E. Woosley, Springer Press, p. 278
42. Van Riper K.A. 1978, ApJ 221, 304
43. Wang L. et al. 2001, Nature, *The Bipolar Ejecta of SN1987A*, submitted
44. Wang L., Howell A., Höflich P., Wheeler J.C. 2001, ApJ, in press
45. Wang, L., Wheeler, J. C., Li, Z. W., & Clocchiatti, A. 1996, ApJ, 467, 435
46. Wang, L., Wheeler, J.C., Höflich, P. 1997, ApJ, 476, 27
47. Yamada S., Janka H.T., Suzuki H. 1999, A&A 344, 533
48. Zwerger T., Müller E. 1997, A&A 320, 209

This figure "fig1.gif" is available in "gif" format from:

http://arXiv.org/ps/astro-ph/0104025v1

This figure "fig2.gif" is available in "gif" format from:

http://arXiv.org/ps/astro-ph/0104025v1

This figure "fig3a.gif" is available in "gif" format from:

http://arXiv.org/ps/astro-ph/0104025v1

This figure "fig3b.gif" is available in "gif" format from:

http://arXiv.org/ps/astro-ph/0104025v1

This figure "fig4.gif" is available in "gif" format from:

http://arXiv.org/ps/astro-ph/0104025v1

This figure "fig5.gif" is available in "gif" format from:

http://arXiv.org/ps/astro-ph/0104025v1